CrystEngComm

Accepted Manuscript

ROYAL SOCIETY OF CHEMISTRY

www.rsc.org/crystengcomm

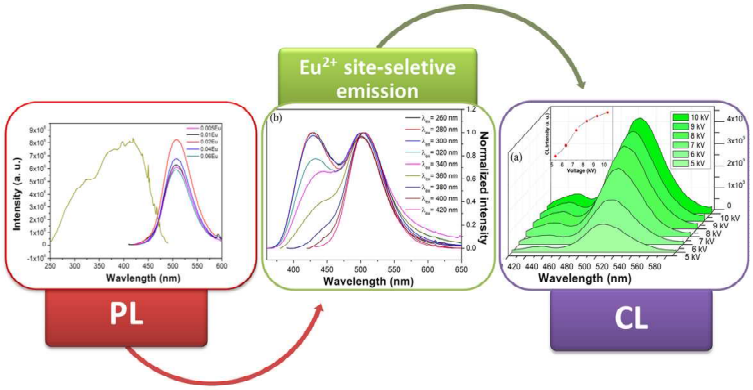

Colour graphic

Text:

Synthesis, electronic structure and photo/cathodoluminescence properties of a green phosphor $NaBaScSi_2O_7:Eu^{2+}$ for LEDs and FEDs

Cite this: DOI: 10.1039/c0xx00000x

www.rsc.org/xxxxxx

ARTICLE TYPE

Electronic structure and photo/cathodoluminescence properties investigation of a green emission phosphor $NaBaScSi_2O_7:Eu^{2+}$ with high thermal stability

Ge Zhu[1], Yurong Shi[1], Masayoshi Mikami[2],Yasuo Shimomura[2], and Yuhua Wang[1*]

Received (in XXX, XXX) Xth XXXXXXXXX 20XX, Accepted Xth XXXXXXXXX 20XX

DOI: 10.1039/b000000x

Abstract

As new light sources for next-generation illumination, white light-emitting diodes (LEDs) have been developed extensively and are commercially available due to their excellent advantages. However, the current white LEDs presently in the market based on the combination of blue chip and yellow phosphor cannot satisfy the need for indoor illumination or some other vivid fields due to the lack of sufficient red spectral component. Here we reported a green phosphor $NaBaScSi_2O_7:Eu^{2+}$ which can be effectively excited by near-ultraviolet chip and emit bright green light with extremely excellent thermal stability. The electronic structure, characteristic photoluminescence and cathodoluminescence properties as well as the thermal quenching properties were investigated in detail. The origin of the desired green luminescence was also determined by analyzing the crystal structure, measuring fluorescence lifetimes and the site-selective excitation and emission spectra. In addition, to investigate its application in field emission displays, the cathodoluminescence (CL) spectra of $NaBaScSi_2O_7:Eu^{2+}$ as a function of accelerating voltage, probe current and the electron radiation time were also measured and discussed in detail. The current results indicate that $NaBaScSi_2O_7:Eu^{2+}$ can serve as a potential green phosphor for application in high-power white LEDs and field emission displays.

1. Introduction

Since Nick Holonyak invented visible light-emitting diodes (LEDs) based on III-V semiconductor p-n junction materials in 1962, LEDs have been developed extensively and are now commercially available with efficacy surpassing those of Edison-style incandescent lamps.[1,2] Comparing with the conventional light sources, white LEDs have more excellent advantages, such as high efficiency, energy-saving, compactness, long operational lifetime and environmental friendly.[3-5] By virtue of these advantages, white LEDs are currently widely used in not only point light sources, but also wide-illumination equipment, back-lighting of liquid-crystal TVs and high-power automotive headlights.[6] The major white LEDs presently in the market are phosphor-converted LEDs (pc-LEDs) constituted of a blue InGaN chip and a yellow phosphor, $(Y,Gd)_3(Al,Ga)_5O_{12}:Ce^{3+}$ ($YAG:Ce^{3+}$).[7] Although this type of white LEDs have been widely used for many years, they are limited to high correlated color temperature (CCT; usually, 6000 K) and low color rending index (CRI; usually, 75),[8-11] which restricts their use in more vivid applications. In order to obtain higher efficiency white LEDs with appropriate CCT and higher CRI, more scientific efforts have therefore focused on using near-ultraviolet (n-UV) or ultraviolet (UV) LED chips coated with blue/green/red tricolor phosphors.[12,13] N-UV pc-LEDs have many potential applications as a result of their excellent CRI, high color tolerance, and high conversion efficiency to visible light.[14] Currently, many illumination applications require significantly higher brightness levels than indicator applications, which has motivated the development of high-power n-UV LEDs.[15] Thus, one of the major challenges for n-UV LEDs is delivering highest efficiency performance at the high current densities and temperatures relevant to high-power operation. As a result, new phosphors with high efficiency and good thermal stability are desperately needed because white light generated by pc-LEDs with a UV/n-UV LED chip strongly depend on the phosphor stability.[16-18] Therefore, there is an urgent tendency to develop new n-UV/UV excitable phosphors with high efficiency and excellent thermal stability. Moreover, as a promising technology in flat panel displays, field emission displays (FEDs) have gained much attention owing to their unique advantages such as thin panel thickness, self-emission, distortion-free images, wide viewing angle, low weight, quick response and low power consumption.[19,20] The same with tri-chromatic white LEDs, the current sulfide-based compound phosphors are also indispensable in FEDs. Thus, increasing attention has been paid to new oxide-based phosphors because of their superior colour richness and good chemical and thermal stabilities compared to sulfides.[21,22] Liu et. al has reported the structure and photoluminescence property of $NaBaScSi_2O_7:Eu^{2+}$.[23] Unlike Liu's work, in this work, we synthesized Eu^{2+} ions doped $NaBaScSi_2O_7$ phosphor and paid more attention to the electronic structure of $NaBaScSi_2O_7$, site occupying situation of Eu^{2+}, site-seletive photoluminescence excitation and emission spectra, as well as the characteristic

temperature-dependent photoluminescence spectra of $NaBaScSi_2O_7$: Eu^{2+}. Moreover, to investigate its potential application in FEDs, the characteristic the cathodoluminescence (CL) spectra of $NaBaScSi_2O_7$:Eu^{2+} as a function of accelerating voltage, probe current and the electron radiation time were also measured and discussed in detail.

2. Experimental

2.1 Synthesis of Phosphors: Powder samples of $NaBa_{1-x}ScSi_2O_7$:xEu^{2+}($0 \le x \le 0.06$) were prepared by a conventional solid-state reaction method. The starting materials are Na_2CO_3 (99%), $BaCO_3$ (99.9%), H_2SiO_3 (99.9%), Sc_2O_3 (99.99%) and Eu_2O_3 (99.99%), used as sources of Na, Ba, Si, Sc and Eu, respectively. 15 *wt*% BaF_2 (99.9%) was used as flux. The stoichiometric raw materials were mixed and ground in an agate mortar in ethanol. Then, the mixtures were preheated in an alumina crucible at 1050 °C for 12 h in air. The resulting powder was thoroughly reground, placed in an alumina crucible inside a tube furnace, and then heated at 1050-1100 °C for 12 h under a reducing atmosphere (5% H_2/95%N_2). Finally, the temperature was slowly lowered to room temperature and cyan-colored (body color) phosphors were obtained.

2.2 Characterization: All the phase structures of samples were characterized by powder X-ray diffraction using a Rigaku diffractometer with Ni-filtered Cu Kα radiation at scanning steps of 0.02° in the 2θ range from 10° to 80°. Diffuse reflectance spectra of samples were collected on finely ground samples by an ultraviolet/visible spectrophotometer using $BaSO_4$ as a reference at steps of 2 nm in the range of 200–700 nm. Excitation and emission spectra were obtained by a FLS-920T fluorescence spectrophotometer with Xe 900 (450 W xenon arc lamp) as the light source. The scanning step was 1 nm. Thermal quenching was tested using a heating apparatus (TAP-02) in combination with PL equipment. The cathodoluminescence properties of the samples were obtained using a modified Mp-Micro-S instrument. All the data were measured at room temperature except for the thermal quenching curves.

The calculations of the electronic structure for $NaBaScSi_2O_7$ were carried out with density functional theory and performed with CASTEP code. The local-density approximations based on density functional theory were chosen for the theoretical basis of the density function. First, the crystallographic data of $NaBaScSi_2O_7$ were used to optimize its crystal structure. The second step was to calculate its density of states for the optimized structure.

3. Results and discussion

3.1 Phase purity analysis

Figure 1 shows a series of XRD patterns of $NaBaScSi_2O_7$:xEu^{2+} ($0 \le x \le 0.06$) phosphors with different doping contents as well as the calculated XRD patterns according to the crystal structure parameters of $NaBaScSi_2O_7$.[24] It can be seen that no detectable impurity phase can be observed in the obtained samples even at high doping concentration. The XRD profiles are well fitted with the calculated XRD patterns, indicating that all the samples are of single phase and the Eu^{2+} ions have been successfully incorporated in the $NaBaScSi_2O_7$ host lattice without changing the crystal structure.

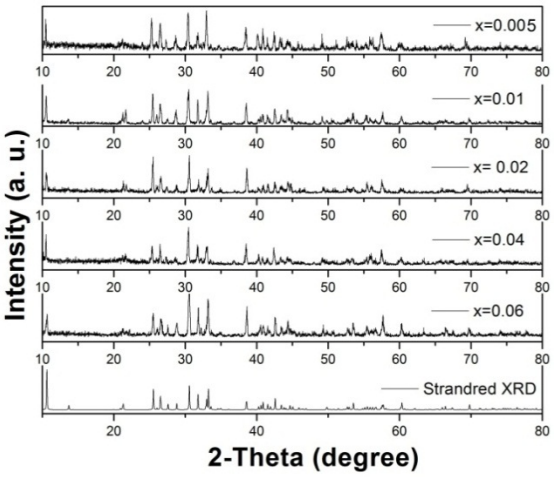

Figure 1 XRD patterns of $NaBaScSi_2O_7$:xEu^{2+} phosphors ($0 \le x \le 0.06$).

3.2 UV-visible DRS spectrum analysis

The UV-visible DRS of undoped $NaBaScSi_2O_7$ and $NaBa_{0.98}Eu_{0.02}ScSi_2O_7$ samples are shown in Figure 2. It can be seen that the DRS of undoped $NaBaScSi_2O_7$ shows little absorption in the visible light range, which agrees well with the observed white body color of the host sample, as shown in Fig. 2. After Eu^{2+} doping, a broad deep valley is observed from 300 to 500 nm, which is due to the strong 4*f*-5*d* transitions of Eu^{2+} at this range and is consistent with the PLE spectra, which will be discussed later. The strong absorption of $NaBa_{0.98}Eu_{0.02}ScSi_2O_7$ in the UV and blue region are also consistent with the green body color of the Eu^{2+} doped samples (the inset of Fig. 2). The inset shows a plot of $[F(R)* h\nu]^{1/2}$ vs. photoenergy hν for $NaBaScSi_2O_7$ host, where F(R) is the Kubelka–Munk function, with $F(R) = (1-R)^2/2R$, and R is the observed reflectance in the DRS. By adopting the methods, the optical band gap energy of $NaBaScSi_2O_7$ is determined to be 4.953 eV by the extrapolation to F(R)=0.

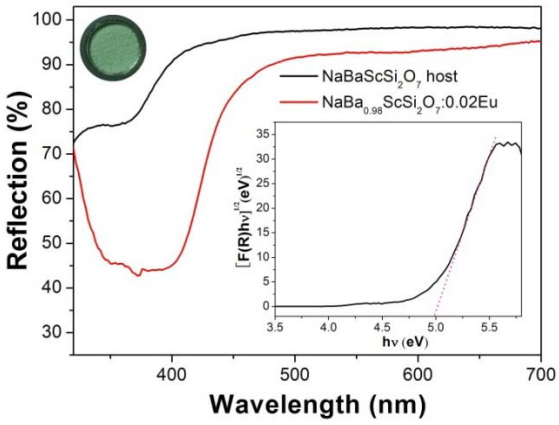

Figure 2 The UV-visible DRS of undoped $NaBaScSi_2O_7$ and $NaBa_{0.98}Eu_{0.02}ScSi_2O_7$ samples; the inset shows a a plot of $[F(R)* h\nu]^{1/2}$ vs. photoenergy hv for $NaBaScSi_2O_7$ host.

Cite this: DOI: 10.1039/c0xx00000x

www.rsc.org/xxxxxx

ARTICLE TYPE

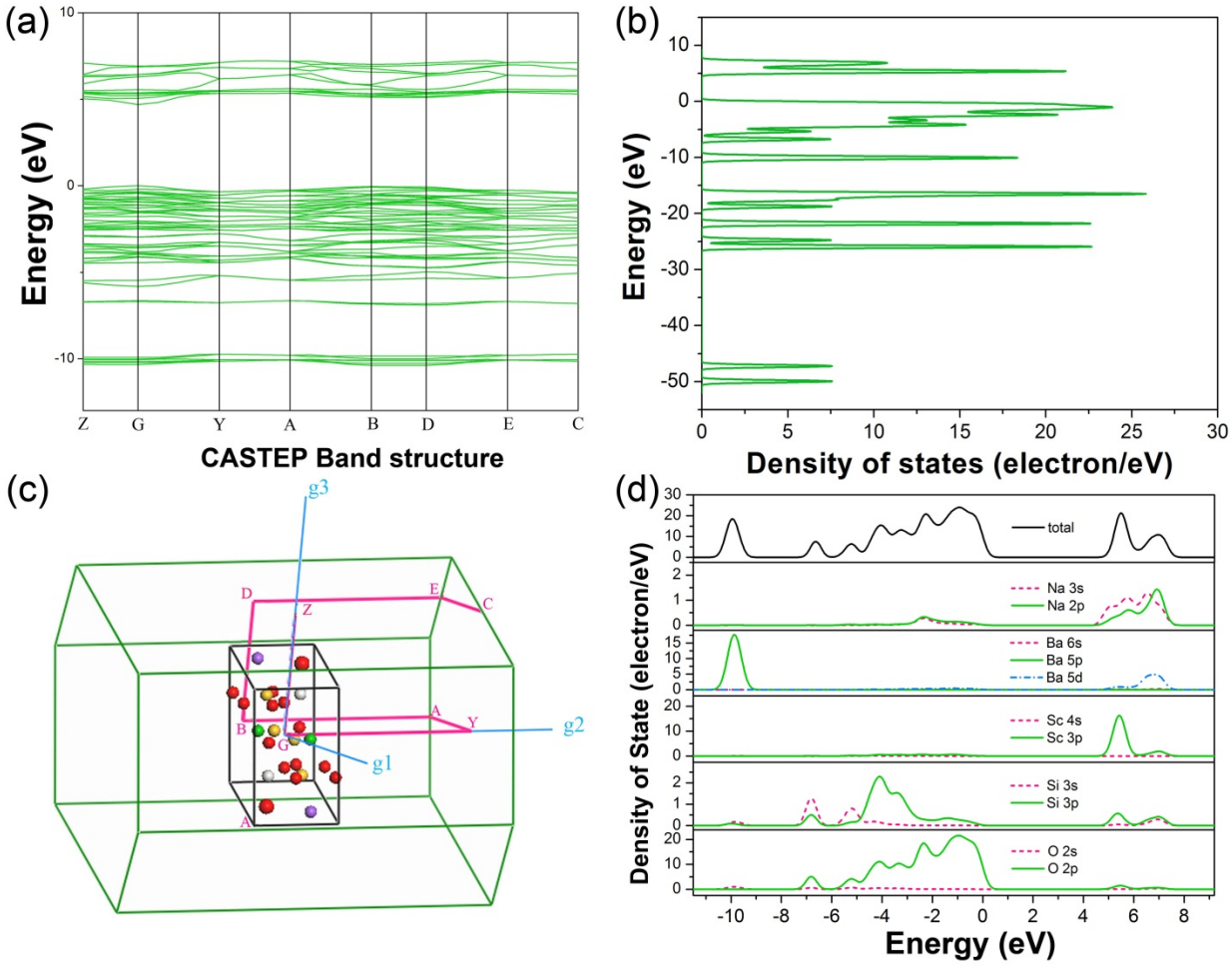

Figure 3 (a) Band structure, (b) density of states, (c) Brillouin zone, (d) total and partial density of states in the range from -11.5 to 9.2 eV.

3.3 Electronic structure of $NaBaScSi_2O_7$ host

The density functional theory calculations of $NaBaScSi_2O_7$ based on crystal structure data are shown in Fig. 4. The local density approximation (LDA) was chosen for the theoretical basis of the density function. This compound possesses an indirect band gap of about 4.462eV with the valence band (VB) maximum at the B point and the conduction band (CB) minimum at the G point of the Brillouin zone. The VB originates predominantly from Si 3*p*, Ba 5*p* and O 2*p* states, whereas the CB is composed mostly of Na 3*s* and 2*d*, Ba 5*d* and Sc 3*d* states. It is expected that the value of the calculated bandgap of about 4.462 eV is similar to the optical band gap energy of $NaBaScSi_2O_7$ through DRS analysis. With such a large band gap, it is expected that the energy levels of the $4f^6 5d \leftrightarrow 4f^7$ transitions of the Eu^{2+} ion in the host lattice of $NaBaScSi_2O_7$ should have small interferences with the valence and conduction bands and $NaBaScSi_2O_7$ host can provide a suitable band gap for Eu^{2+} to act as emission center.[25]

3.4 Photoluminescence properties of $NaBaScSi_2O_7:Eu^{2+}$

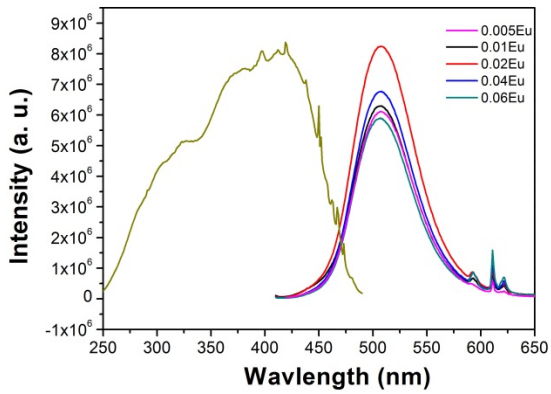

Figure 4 The PLE spectrum of $NaBaScSi_2O_7$: $0.02Eu^{2+}$ phosphor monitored at 506 nm. The PL spectra of $NaBaScSi_2O_7$: xEu^{2+} ($0.005 \leq x \leq 0.06$) phosphors at 406 nm excitation.

Figure 4 illustrates the PLE and PL spectra of Eu^{2+} doped

$NaBaScSi_2O_7$ phosphor. When monitored at 506 nm, the PLE spectrum shows a broad band of 250 to 500 nm and has strong intensity around 400-410 nm. The strong excitation in 400-410 nm matches well with the current n-UV LED GaN chips, which indicates that $NaBaScSi_2O_7$:Eu^{2+} phosphor can be a promising candidate for n-UV pumped white light emitting diodes. The unresolved broad band is assigned to the transition between the ground-state $4f^7$ and the crystal-field split $4f^6 5d$ configuration of Eu^{2+}. Under 406 nm excitation, the $NaBaScSi_2O_7$: Eu^{2+} phosphor exhibits an intense green emission and the corresponding emission spectrum consists of a broad emission band centered at 508 nm due to the electric-dipole-allowed transition from the $5d$ excited state to the $4f$ ground state of the Eu^{2+}.[26] In order to further investigated the luminescence properties, a series of Eu^{2+} with different doping content samples $NaBaScSi_2O_7$:xEu^{2+} ($0.005 \leq x \leq 0.06$) are synthesized. As we can see from the PL spectra, as increasing Eu^{2+} contents, the PL intensity was found to increase gradually until $x>0.02$, reaching to concentration quenching. That is, when the Eu^{2+} ions content increases, more and more Eu^{2+} ions pair or aggregate with others, efficient resonant energy transfer between Eu^{2+} ions and a fraction of migration to distant luminescent killer of quencher occur, leading to the luminescence quenching. We also compared $NaBaScSi_2O_7$:$02Eu^{2+}$ with the commercial green phosphor and the result shows that the emission intensity of $NaBaScSi_2O_7$:xEu^{2+} is as high as 89% of the commercial-green phosphor (LMS520B). In addition, the full width at half maximum (FWHM) of $NaBaScSi_2O_7$:$0.02Eu^{2+}$ is measured to be about 70 nm and the emission band covers both blue and green region, even extends to yellow region in the spectrum. This means, to realize the fabrication of white light LEDs lamp, we only need to mix $NaBaScSi_2O_7$:Eu^{2+} with a red phosphor instead of traditionally mixing three color phosphors. This cannot only effectively decrease the loss due to the reabsorption and get high luminous efficacy, but also can simplify the fabrication process greatly.[27]

Figure S1 presents the crystal structure diagram of monoclinic $NaBaScSi_2O_7$ with space-group symmetry P21/m. The crystal structure of $NaBaScSi_2O_7$ is a three-dimensional framework consisting of tetrahedra and octahedral groups, which are based on the isolated Si_2O_7 group connected octahedrally coordinated Sc cations, nine-coordinated Ba cations and eight-coordinated Na cations. Table S1 lists the effective ionic radii of cations (Na, Ba) with different coordination numbers.[28] For eight-coordinated Na^+ and nine-coordinated Ba^{2+} cations, the effective ionic radii are 1.18 and 1.47 Å, respectively. The effective ionic radii for those of Eu^{2+} are 1.25 and 1.30 Å, respectively. So based on comparing of the effective ionic radii of cations with different coordination numbers, we propose that Eu^{2+} ions are expected to randomly occupy the Ba^{2+} and Na^+ sites in the host structure. Generally, if Eu^{2+} occupy only one cation site, the emission spectrum is symmetrical.[29] It should be noted that the emission spectrum presents a broad band with a maximum wavelength at about 506 nm and a tail on the long-wavelength side. This phenomenon seems to be very interesting but we think it should be related to the *f-f* transitions emission of the unreduced Eu^{3+} in the sample rather than the double-emission of Eu^{2+} from two sites. The little unreduced Eu^{3+} emission can also be detected in the emission spectrum (the small emission at about 590nm and 612 nm, which are attributed to the $^5D_0$-$^7F_1$ and $^5D_0$-$^7F_2$ transitions of Eu^{3+}).

3.5 Site-selective luminescence property and site occupying investigation

In order to further investigate and prove the Eu^{2+} occupying situation in $NaBaScSi_2O_7$, we prepared the very low content Eu^{2+} ions (1 mol‰) doped $NaBaScSi_2O_7$ sample and investigated its characteristic luminescence properties. Fig. 5a shows the excitation spectra of $NaBaScSi_2O_7$:$0.001Eu^{2+}$ monitored at different excitation wavelength. When monitored at 427 nm, the excitation spectrum exhibits a broad excitation band centred at about 300 nm, corresponding to the $4f^7$ to $4f^6 5d$ transitions of Eu^{2+}. However, when the monitoring wavelength is fixed at 506 nm, the excitation spectrum shows not only the excitation band at 300 nm but also a stronger excitation band centred at about 400 nm, which is similar with the excitation spectrum in Fig. 4. The difference indicates that there may be occupying not only one cation site of Eu^{2+} in $NaBaScSi_2O_7$. Then we measure the site-selective emission spectra by exciting the sample at different excitation wavelength, as shown in Fig. 5b. It is clearly seen that the emission spectra consist of two emission bands centred at about 427 nm and 505 nm. When excited at 260 and 280 nm, the emission band centred at 427 nm is dominate while with increasing the excitation wavelength, the former emission band (427 nm) becomes weaker and the later emission band (505 nm) becomes stronger and stronger, which is due to the site-selective excitation from two different sites (eight-coordinated Na and nine-coordinated Ba) in Eu^{2+} doped $NaBaScSi_2O_7$ and this is also corresponding to its excitation spectra as shown in Fig. 5a. In order to further verify the occupancy ascription of the two emission bands, the empirical relation between the energy position of the Eu^{2+} emission and the local structure in various compounds by Van Uitert was employed as eqn. (1),[30]

$$\mathrm{E\ (cm^{-1})} = \mathrm{Q}\left[1 - \left(\frac{V}{4}\right)^{\frac{1}{V}} 10^{-\emptyset}\right] \qquad (1)$$

Where $\emptyset = (\mathrm{n\ ea\ r})/80$, E is the position for the Eu^{2+} ion emission peak, Q is the position in energy for the lower d-band edge for the free Eu^{2+} ion (34000 cm^{-1}), V is the valence of the Eu^{2+} ion (V=2), n is the number of anions in the immediate shell about the Eu^{2+} ion, ea is the electron affinity of the atoms that form anions (eV), and r is the radius of the host cation replaced by the Eu^{2+} ion (Å). For ea value in the present host is very complex and hardly to be obtained the specific data, but it is constant in the same host. Thus, according to Uitert's report, the value of E is directly proportional to the product of n and r. Based on the data in Table S1, the product of n and r for Na^+ is 9.44 and that for Ba^{2+} is 13.24 in $NaBaScSi_2O_7$. So we can draw a conclusion that the former band centered at 427 nm is attributed to the 5d-4f transitions of Eu^{2+} occupying Ba^{2+} sites with nine-coordination, and the later emission band centered at 505 nm is attributed to the 5d-4f transitions of Eu^{2+} occupying Na^+ site with eight-coordination, respectively. In order to further prove that Eu^{2+} occupying both Na^+ and Ba^{2+} sites in the current $NaBaScSi_2O_7$ host, the luminescence decay curves were measured by exciting at 300 nm and monitoring at 427 and 505 nm, respectively. The results were shown in Fig. 5c and 5d. The corresponding luminescent decay times can be fitted by a double

Cite this: DOI: 10.1039/c0xx00000x

www.rsc.org/xxxxxx

ARTICLE TYPE

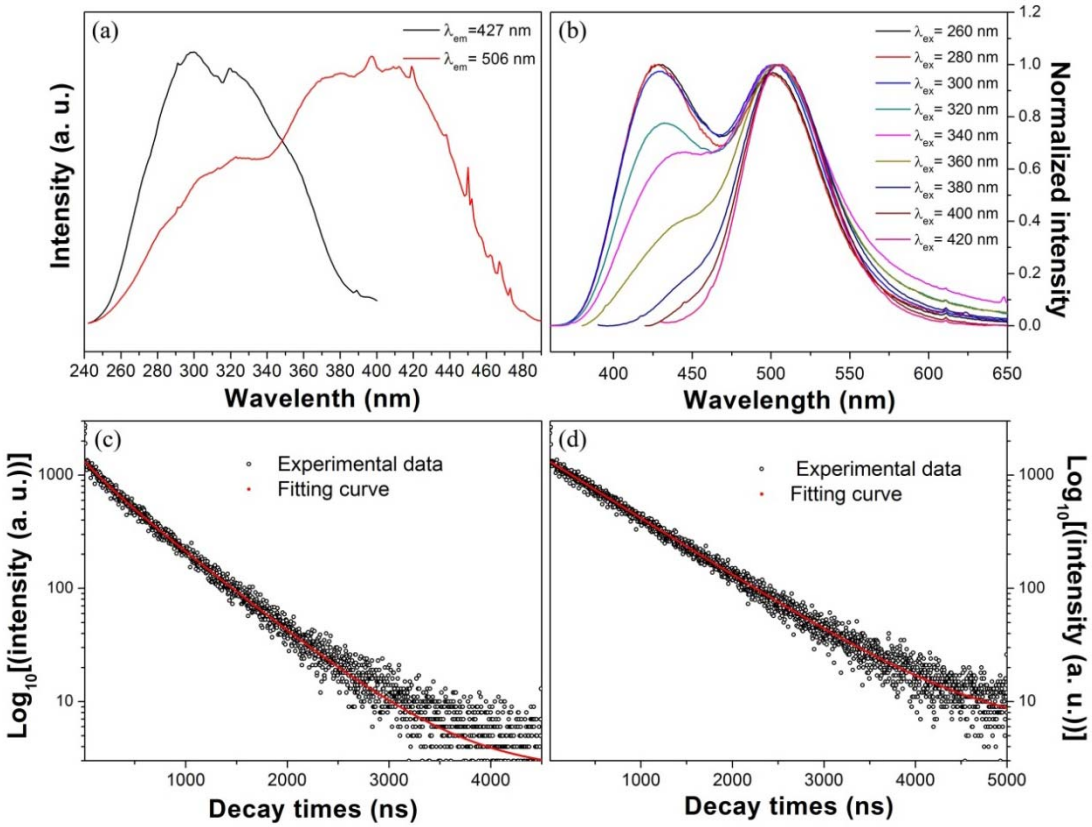

Figure 5 (a) The excitation spectra of $NaBaScSi_2O_7$:0.001Eu^{2+} monitored at 427 and 506 nm; (b) The emission spectra of $NaBaScSi_2O_7$:0.001Eu^{2+} excited at different excitation wavelength; (c) The luminescence lifetimes of $NaBaScSi_2O_7$:0.001Eu^{2+} excited at 300 nm and monitored at 427 nm; (d) The luminescence lifetimes of $NaBaScSi_2O_7$:0.001Eu^{2+} excited at 300 nm and monitored at 505 nm.

-exponential mode and the average decay time τ can be determined by the formula,[31]

$$\tau = \frac{A_1\tau_1^2 + A_2\tau_2^2}{A_1\tau_1 + A_2\tau_2} \quad (2)$$

where A_1 and A_2 are constant, τ_1 and τ_2 are the two exponential component of the decay time. The detailed fitting parameters are given in Table S2. On the basis of eqn. (2) and the measured decay curves, the average lifetime of Eu^{2+} in $NaBaScSi_2O_7$ can be calculated to be 578 and 878 ns, respectively. The dual-exponential curve fitting is due to the large spectra overlap of the two emission bands and can also support that Eu^{2+} occupying both of Na^+ and Ba^{2+} sites in $NaBaScSi_2O_7$.

3.5 Thermal quenching property investigation

For application in high power LEDs, the thermal quenching property is one of the important technological parameters for phosphors because it has considerable influence on the light output and color rendering performance. The temperature dependent emission spectra for $NaBaScSi_2O_7$:0.02Eu^{2+} excited at 406 nm were measured and illustrated in Fig. 5(a). For comparison, the thermal quenching properties of the commercial green phosphor (com-green LMS520B) have also been measured. As we can see, both the intensity of the $NaBaScSi_2O_7$:0.02Eu^{2+} phosphor and the com-green phosphor decrease gradually as the temperature increases and the thermo stability of $NaBaScSi_2O_7$:0.02Eu^{2+} is found to be much better than the com-green phosphor LMS520B. As shown in the inset, when the temperature was increased to 260 °C, the emission intensity of $NaBaScSi_2O_7$:0.02Eu^{2+} dropped to only 75% of its initial intensity, while that of the com-green phosphor decreased to 15%. The excellent thermal stability strongly supported that $NaBaScSi_2O_7$:0.02Eu^{2+} phosphor is suitable for application in high-power LEDs. The thermal degradation of $NaBaScSi_2O_7$:0.02Eu^{2+} phosphors can be attributed to the nonradiative transition from the excited state ($4f^6 5d^1$) to the ground state ($4f^7 5d^0$). As shown in Fig. 6c, at room temperature, the radiative transition from nearly the bottom of the excited state to the ground state occurs (line CD and EF) and no temperature dependence is observed. With increasing the temperature, the

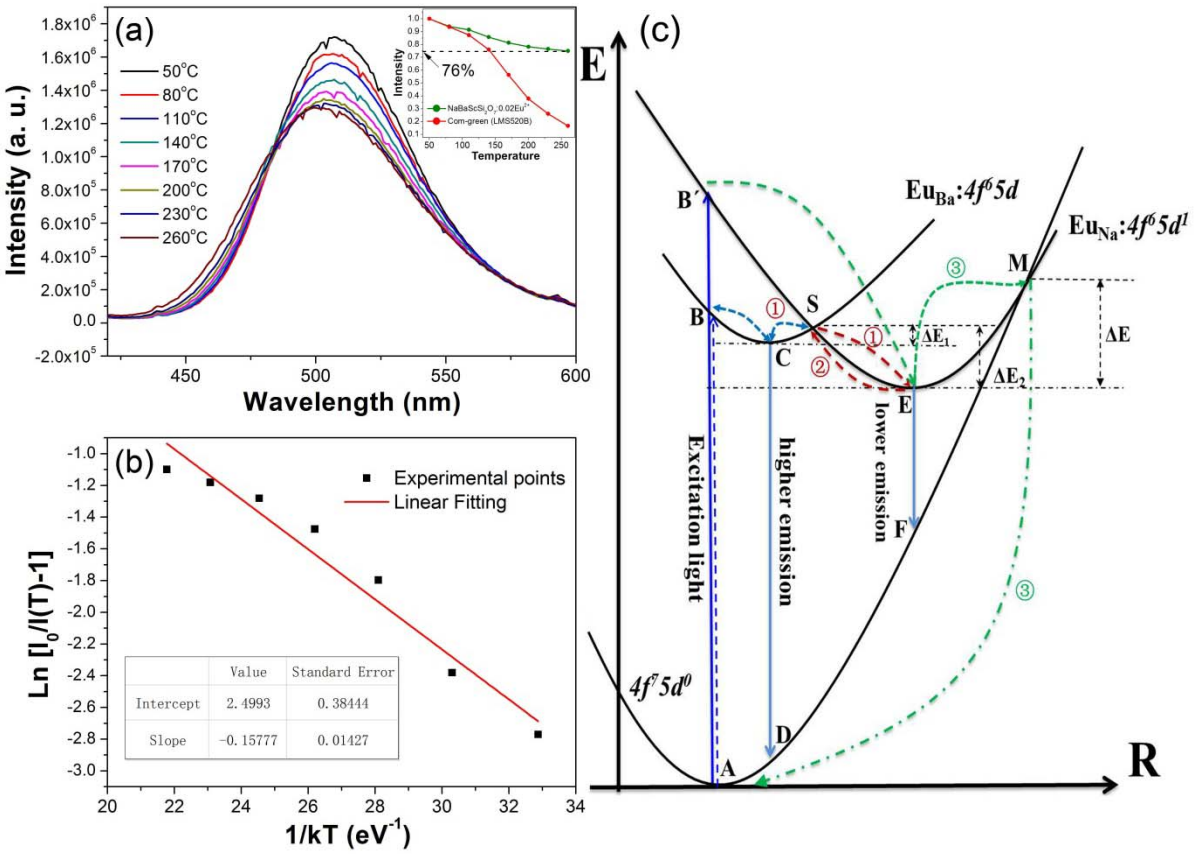

Figure 6 (a) The temperature dependent emission spectra of $NaBaScSi_2O_7$:0.02Eu^{2+}, the inset shows the thermal stability comparison between $NaBaScSi_2O_7$:0.02Eu^{2+} and the com-green phosphor (LMS520B); (b) The activation energy (ΔE) for thermal quenching of $NaBaScSi_2O_7$:0.02Eu^{2+} excited at 406 nm; (c) Configurational coordinate diagram of the ground state ($4f^75d^0$) and two split excited states (Eu_{Ba} $4f^65d$ and Eu_{Na} $4f^65d$)

excited state obtains thermal energy and overcome the energy barrier ΔE and cross-over to the ground state (through process ③) and as a result nonradiative transition becomes more dominant. As a result, the process enhances with increasing temperature and the luminescence intensity becomes weaker at high temperatures.[32] In order to interpret the relationship of emission intensity with temperature and to calculate the activation energy (ΔE) for thermal quenching, the Arrhenius equation was fitted to the thermal quenching data,[33]

$$I(T) = I_0[1 + Aexp(-\Delta E/kT)]^{-1} \qquad (3)$$

Where I is the intensity at a given temperature, I_0 is the initial intensity, k is the Boltzmann's constant, T is temperature and ΔE is the activation energy for thermal quenching process. As displayed in Fig. 6b, the experimental data can be well fitted by a linear fit, indicating that the temperature quenching process complies well with the Arrhenius-type activation model. Then the activation energy ΔE of thermal quenching can be estimated from the slope of the ln{[I_0/I(T)]-1}vs 1/kT plot and is calculated to be 0.16 eV.

It can be noted that the emission spectra show a blue-shift when the temperature increases. Generally, the luminescence shows characteristic temperature dependence: the emission peak shifts to a lower energy (red-shift) as the temperature increases.[34,35] This behavior has been explained by the Varshni equation,[36]

$$E(T) = E_0 - \frac{aT^2}{T+b} \qquad (4)$$

where E(T) is the energy difference between excited states and ground states at a temperature T, E_0 is the energy difference at 0 K, and a and b are fitting parameters. At a high temperature, the bond lengths between the luminescent center (e.g., Eu^{2+}) and its coordination ions increase, resulting in the decreased crystal field. Also the symmetry of luminescent center is distorted so that John–Teller effect is dominant. The two effects cause to splitting of degenerate excited state or ground state, which causes the decrease of the transition energy and the red-shifted of the emission peak with the increase of temperature.[37,38] However, the emission spectra of $NaBaScSi_2O_7$:0.02Eu^{2+} phosphor are found to

Cite this: DOI: 10.1039/c0xx00000x

www.rsc.org/xxxxxx

ARTICLE TYPE

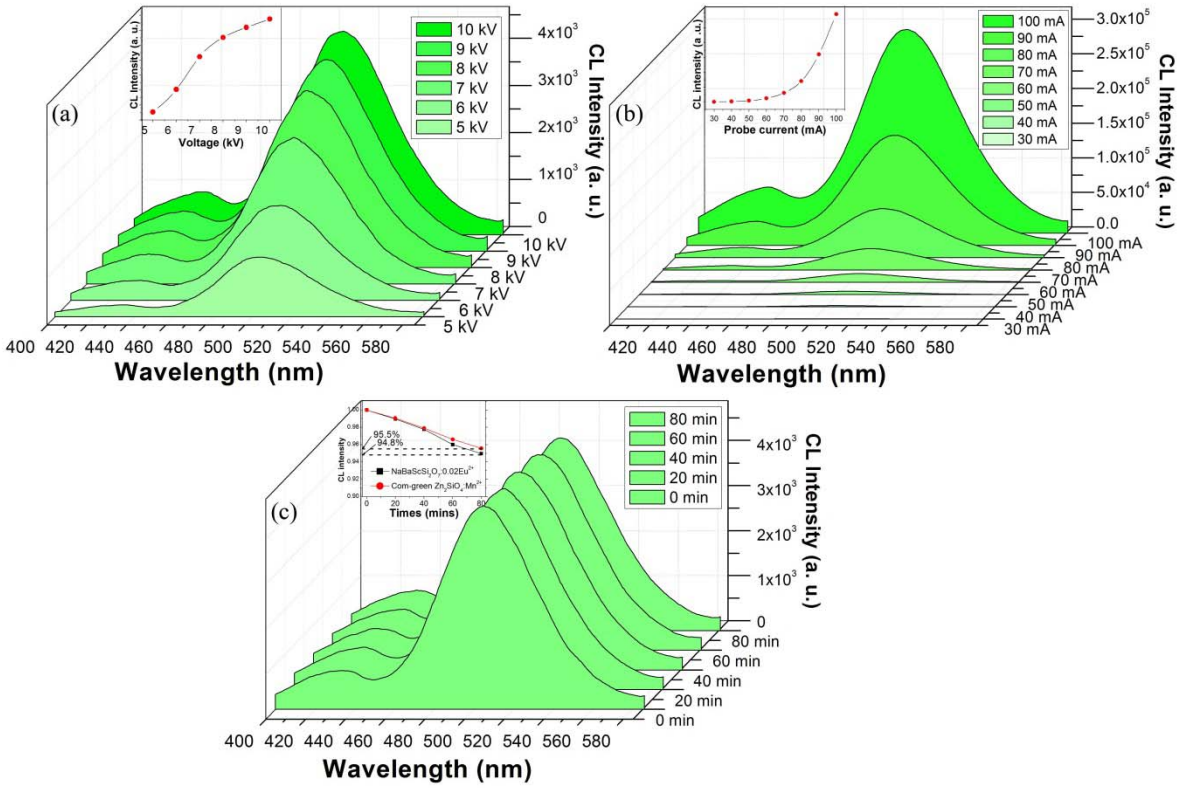

Figure 7 CL intensity of $NaBaScSi_2O_7$:0.02Eu^{2+} phosphor as a function of (a) accelerating voltage, (b) probe current and (c) electron radiation time; the insets clearly show their relationship.

be blue-shifted with increasing temperature. This cannot be interpreted by eqn. (4) for the temperature dependence redshift behavior and we think to account for this observation it should be considered that thermally active phonon-assisted tunneling from the excited states of low-energy emission band to the excited states of high-energy emission band in the configuration coordinate diagram occurs, as illustrated in Fig. 6c.[36, 37] It has been proved that there should be two different Eu^{2+} sites (Eu_{Ba} and Eu_{Na}) in the $NaBaScSi_2O_7$ host. Since Eu_{Ba} and Eu_{Na} experience different crystal field strengths, the $4f^65d^1$ excitation states are located at different energy levels, and the excitation state transformed to the ground state with different energy values when they were excited by the excitation light from 240 to 480 nm.[36,39] At low temperature, the barrier ΔE_1 can be overcome and the low-energy emission (from Eu_{Na}) is dominant (through process ①). At higher temperature, the thermal back-transfer over the barrier ΔE_1 is possible, and consequently the higher energy emission (from Eu_{Ba}) is dominant (through process ②). Thus, the blue-shift behavior is observed with increasing temperature. [36, 40]

3.6 Cathodoluminescence property investigation

The cathodoluminescence (CL) properties of $NaBaScSi_2O_7$:0.02Eu^{2+} phosphor have been measured, in order to explore the potential of $NaBaScSi_2O_7$:0.02Eu^{2+} as a novel green phosphors in the development for FED systems, as shown in Fig. 7. Under the low voltage electron beam excitation, the pure $NaBaScSi_2O_7$:0.02Eu^{2+} phosphor mainly showed a broad green emission centered at about 508 nm and a small weak blue emission at about 430 nm, attributed to the 5*d*-4*f* transitions of Eu^{2+} occupying Na^+ and Ba^{2+} sites, respectively, which has been discussed before. The double emission bands in $NaBaScSi_2O_7$:0.02Eu^{2+} under electron-beam excitation further supported that Eu^{2+} ions were occupying different sites in $NaBaScSi_2O_7$, which is agreement with the previous analysis. The little red-shift of the emission bands compared with the photoluminescence spectra (Fig. 4 and Fig. 5b) might be due to the energy level structures of vacancy defects and the different excitation mechanism.[41] The CL emission intensities of the $NaBaScSi_2O_7$:0.02Eu^{2+} sample have been investigated as a function of the accelerating voltage and the filament current as shown in Fig. 7a and 7b. As the anode voltages increased and kept the anode current density as 50 μA/cm^2, the CL intensity was found to be gradually increased with applied voltage increasing from 5.0 to 10.0 kV (inset of Fig. 7a). Similarly, under a 5 kV electron-beam excitation, the CL intensity also increases

with increasing the filament current from 30 to 100 mA (inset of Fig. 7b). The increase of the CL intensity with an increase in the electron energy should be attributed to the deeper penetration of the electrons into the phosphor body and the larger electron-beam current density, which has been discussed in many places.[42-44] The degradation property for phosphor is very important for FED application. Thus, we also investigated the degradation behavior of $NaBaScSi_2O_7$:0.02Eu^{2+} samples under continuous low-voltage electron-beam excitation and illustrated in Fig. 7c. The measurement was carried out under the condition of anode voltage of 5 kV and anode current density of 50 μA/cm^2. For comparison, the degradation property of the commercial green (com-green) phosphor Zn_2SiO_4:Mn^{2+} (type: P1-GIS) was also measured. The inset of Fig. 7c gives the normalized CL emission intensity of the two phosphors as a function of electron radiation time. It could be seen that $NaBaScSi_2O_7$:0.02Eu^{2+} has a good degradation property. After being bombarded by persistent electron beam for 80 mins, it could retain about 94.6% of the initial intensity, and the com-green Zn_2SiO_4:Mn^{2+} could keep about 95.5% of the initial value. This result is also much better than other commercial green phosphor such as ZnS: Ag, Cl (dropped to about 55%).[46] The degradation of the CL intensity may be due to the accumulation of carbon at the surface during electron radiation. During continuous electron radiation, the graphitic carbon will accumulate on the surface of phosphors and caused a well-known effect as carbon contamination, which will exacerbate surface charging, and thus lower the CL intensity.[45-47] The better degradation properties of $NaBaScSi_2O_7$:0.02Eu^{2+} is apparently due to the stable nature of $NaBaScSi_2O_7$ host, which is also consistent with its excellent thermal stability property.[45]

Conclusion

In summary, we have successfully developed a green emitting phosphor $NaBaScSi_2O_7$:0.02Eu^{2+} for high-power n-UV LEDs and FEDs. The phosphor can be efficiently excited over a broad spectral range from 250 to 450 nm and give bright green emission centered at about 506 nm. The photoluminescence excitation and emission spectra are investigated. The origin of the green emission was also determined by analyzing the crystal structure, fluorescence lifetime and site-selective emission spectra, which was proved to be the 5*d*-4*f* transitions of Eu^{2+} occupying Na^+ sites. Temperature dependence of luminescence demonstrates that $NaBaScSi_2O_7$: Eu^{2+} has excellent thermal stability. With increase in temperature, the Eu^{2+} emission wavelength is found to blue-shift slightly, which can be attributed to the thermally active phonon-assisted excitation process from lower energy sublevel to higher-energy sublevel in the excited states of Eu^{2+}. The characteristic cathodoluminescence properties were also investigated with good degradation property. The current results indicated that $NaBaScSi_2O_7$: Eu^{2+} can serve as a potential green phosphor for NUV light pumped white LEDs and FEDs.

Acknowledgments

This work is supported by National Natural Science Funds of China (Grant No. 51372105) and Specialized Research Fund for the Doctoral Program of Higher Education (no. 20120211130003)

Notes and references

[a] *Department of Materials Science, School of Physical Science and Technology, Lanzhou University, Lanzhou, 730000, China. Key Laboratory for Magnetism and Magnetic Materials of the Ministry of Education, School of Physical Science and Technology, Lanzhou University, Lanzhou 730000, China. Fax: +86-931-8913554; Tel: +86-931-8912772; E-mail: wyh@lzu.edu.cn*
[b] *Mitsubishi Chemical Group Science and Technology Research Center, Yokohama 227-8502, Japan*

† Electronic Supplementary Information (ESI) available: [details of any supplementary information available should be included here]. See DOI: 10.1039/b000000x/

1. N. Holonyak Jr, *Am. J. Phys*., 2000, **68**, 864.
2. J. Ryou and R. Dupuis, *Opt. Express*, 2011, **19**, A898.
3. EF. Schubert and JK. Kim, *Science*, 2005, **308**, 1274.
4. S. Pimputkar, JS Speck, SP. DenBaars and S. Nakamura, *Nature Photon*, 2009, **3**, 180.
5. S. Ye, F. Xiao, Y. X. Pan, Y. Y. Ma and Q. Y. Zhang, *Mater. Sci. Eng. Rep*., 2010, **71**, 1.
6. H. Yamamoto, *Proc SPIE*, 2010, **7598**, 759808.
7. (a) H. A. Höppe, Angew. Chem., 2009, 121, 3626; (b) H. A. Höppe, *Angew. Chem. Int. Ed*., 2009, **48**, 3572.
8. AA. Setlur, *Electrochem. Soc. Interface*, 2009, **18**, 32.
9. M. Roushan, X. Zhang and J. Li, *Angew. Chem. Int. Ed*., 2012, **124**, 451.
10. M. Roushan, X. Zhang and J. Li, *Angew. Chem. Int. Ed*., 2012, **51**, 436.
11. A. A. Setlur, W. J. Heward, Y. Gao, A. M. Srivastava, R. G. Chandran and M. V. Shankar, *Chem. Mater*., 2006, **18**, 3314.
12. S. E. Brinkley, N. Pfaff, K. A. Denault, Z. Zhang, H. T. Hintzen, R. Seshadri, S. Nakamura and S. P. DenBaars, *Appl. Phys. Lett*., 2011, **99**, 241106.
13. (a) Y. Uchida and T. Taguchi, *Opt. Eng*., 2005, **44**, 124003.; (b) C. C. Lin, Z. R. Xiao, G. Y. Guo, T. S. Chan and R. S. Liu, *J. Am. Chem. Soc*., 2010, **132**, 3020.
14. E. Radkov, R. Bompiedi, A. M. Srivastava and A. A. Setlur, C.Becker, *Proc. SPIE-Int. Soc. Opt. Eng*., 2004, **5187**, 171.
15. M. H. Crawford, *Journal of Selected Topics in Quantum Electronics*, 2009, **15**, 1028.
16. W. B. Im, N. N. Fellows, S. P. DenBaars and R. Seshadri, *J. Mater. Chem*. 2009, **19**, 1325.
17. Y. C. Yang and S. L. Wang, *J. Am. Chem. Soc*. 2008, **130**, 1146.
18. W. Ki and J. Li, *J. Am. Chem. Soc*. 2008, **130**, 8114.
19. S. Zhang, H. B. Liang, Y. W. Liu, Y. F. Liu, D. J. Hou, G. B. Zhang and J. Y. Shi, *Opt. Lett*., 2012, **13**, 2511.
20. G. Li, Z. Hou, C. Peng, W. Wang, Z. Cheng, C. Li, H. Lian and J. Lin, *Adv. Funct. Mater*., 2010, **20**, 3446.
21. G. Li, D. Geng, M. Shang, C. Peng, Z. Cheng and J. Lin, *J. Mater. Chem*., 2011, **21**, 13334;
22. M. Xie, H. Liang, Y. Huang and Y. Tao, *Opt. Express*, 2012, **20**, 15891.
23. C. Liu Z. Xia, Z. Lian, J. Zhou and Q. Yan, *J. Mater. Chem. C*, 2013, **1**, 7139.
24. M. Wierzbicka-wieczorek, *The Canadian Mineralogist*, 2010, **48**, 51.
25. Y. Li, Y. Fang, N. Hirosaki, R. Xie, L. Liu, T. Takeda and X. Li, *Materials*, 2010, **3**, 1692.
26. G. Lee, J. Y. Han, W. B. Im, S. H. Cheong and D. Y. Jeon, *Inorg. Chem*. 2012, **51**, 10688.
27. N. Narendran, N, Maliyagoda, L. Deng, R. M. Pysar, *Proc. SPIE, 2001, 4445, 137.*
28. R. D. Shannon, *Acta Cryst*., 1976, **A32**, 751.
29. Y. Wen, Y. Wang, B. Liu, F. Zhang and Y. Shi, *Functional Materials Letters*, 2012, **5**, 1250048.
30. L. G. Van Uitert, *J. Lumin*., 1984, **29**, 1.
31. N. Ruelle, M. P. Thi, and C. Fouassier, *Jpn. J. Appl. Phys*., 1992, **31**, 2786.
32. J. Y. Han, W. B. Im, G. Lee and D. Y. Jeon, *J. Mater. Chem*., 2012, **22**, 8793.

Cite this: DOI: 10.1039/c0xx00000x

www.rsc.org/xxxxxx

ARTICLE TYPE

33. V. Bachmann, A. Meijerink, C. Ronda, *J. Lumin*., 2009, **129**, 1341.
34. Y. Huang, J. Gan, R. Zhu, X. Wang and H. J. Seo, *J. Electrochem. Soc*., 2011, **158**, J334.
35. V. B. Mikhailik, H. Kraus, D. Wahl, M. Itoh, M. Koike and I. K. Bailiff, Phys. Rev. B., 2004, **69**, 205110.
36. Y. P. Varshini, *Physica*, 1967, **34**, A149.
37. S. Shionoya, W. M. Yen, *Phosphor Handbook*, CRC Press, New York, 1998.
38. J. S. Kim, Y. H. Park, S. M. Kim, J. C. Choi, H. L. Park, *Solid State Commun.*, 2005, **133**, 445.
39. Z. Xia, X. Wang, Y. Wang, L. Liao and X. Jing, *Inorg. Chem*., 2011, **50**, 10134.
40. Y. Huang, J. Gan, R. Zhu, X. Wang and H. J. Seo，*J. Electrochem. Soc*., 2011, **158** (11), J334.
41. X. M. Liu and J. Lin, *J. Mater Chem*., 2008, **18**, 221.
42. F. L. Zhang, S. Yang, C. Stoffers, J. Penczek and P. N. Yocom, *Appl. Phys. Lett*., 1998, **72**, 2226.
43. M. Shang, G. Li, D. Yang, X. Kang, C. Peng, Z. Cheng and J. Lin, *Dalton Trans*., 2011, **40**, 9379.
44. N. Zhang, C. Guo and H. Jing, *RSC Adv.*, 2013, **3**, 7495.
45. X. Xu, J. Chen, S. Deng, N. Xu, H. Liang, Q. Su and Jun Lin, *Opt. Express*, 2012, **20**, 17701.
46. X. G. Xu, J. Chen, S. Z. Deng, N. S. Xu and J. Lin, *J. Vac. Sci. Technol*., 2010, **28**, 490.
47. J. J. Hren, in Principles of Analytical Electron Microscopy, edited by D.C. Joy, A. D. Romig, and J. I. Goldstein (Plenum, New York, 1986), p. 353.